

ORIGINAL ARTICLE

Open Access



Progressive Failure Analysis of Composite/Aluminum Riveted Joints Subjected to Pull-Through Loading

Yuxing Yang¹, Yongjie Bao^{1*}, Xueshu Liu², Jinlong Wang¹ and Fengming Du¹

Abstract

Out-of-plane mechanical properties of the riveted joints restrict the performance of the wing box assembly of airplane. It is necessary to investigate the pull-through performance of the composite/metal riveted joints in order to guide the riveting design and ensure the safety of the wing box assembly. The progressive failure mechanism of composite/aluminum riveted joint subjected to pull-through loading was investigated by experiments and finite element method. A progressive damage model based on the Hashin-type criteria and zero-thickness cohesive zone method was developed by VUMAT subroutine, which was validated by both open-hole tensile test and three-point bending test. Predicted load-displacement response, failure modes and damage propagation were analysed and compared with the results of the pull-through tests. There are 4 obvious characteristic stages on the load-displacement curve of the pull-through test and that of the finite element model: first load take-up stage, damage stage, second load take-up stage and failure stage. Relative error of stiffness, first load peak and second load peak between finite element method and experiments were 8.1%, -3.3% and 10.6%, respectively. It was found that the specimen was mainly broken by rivet-penetration fracture and delamination of plies of the composite laminate. And the material within the scope of the rivet head is more dangerous with more serious tensile damages than other regions, especially for 90° plies. This study proposes a numerical method for damage prediction and reveals the progressive failure mechanism of the hybrid material riveted joints subjected to the pull-through loading.

Keywords Composite/metal joints, Riveted joints, Pull-through test, Progressive damage model

1 Introduction

With the continuous improvement of energy-saving, emission-reduction and lightweight requirements around the world, composite materials have gradually become one of the major industrial manufacturing materials [1, 2], which has the advantages of light weight, high stiffness-to-weight ratio, high strength-to-weight ratio and

superior resistance to fatigue degradation [3–6]. Nowadays, more and more complicated composite parts are designed and applied in aerospace industry and marine industry [7, 8], which makes it a big problem to guarantee connecting performance of the joints during wing box assembling for airplane. Riveting is one of the widely-used connecting methods in composite components assembly for airplane [9–12], which has the advantages of stable and reliable connection performance, easy automation, wide application range, high reproducibility and fast joining processes [13–15]. As has been reported, Italian-based *BBA Srl* has manufactured a unique riveting method for carbon fiber composite materials, Bulge Control Technology, which can be used where the hole in the workpiece is up to 0.5 mm greater than the rivet

*Correspondence:

Yongjie Bao
yongjie@dlmu.edu.cn

¹ Marine Engineering College, Dalian Maritime University, Dalian 116026, China

² School of Automotive Engineering, Dalian University of Technology, Dalian 116024, China

nut external size [16]. However, riveting requires hole drilling so that reducing the strength of the connected parts, especially for composite laminates [17, 18]. Meanwhile, mechanical properties of riveting, especially static strength and fatigue life, is influenced by both geometrical features, die pressure, shape [19], etc. Therefore, it is necessary to investigate the bearing performance of the riveted joints in order to guide the riveting design and ensure the safety of the joints.

A lot of research works have been done about composite riveting or composite/metal riveting, including joints load distribution and joint damage prediction, etc. Sathiya et al. [20, 21] investigated a composite/metal lap joints for the rivet load distribution and life estimation. It was found that the load shared by the rivet rows in a composite/metal lap joints was not symmetric and therefore are more susceptible to cracking and subsequent failure as the unequal distribution can cause some of the rivet loads to be high. Solmaz et al. [22] used the progressive damage model to analyse the woven-type glass fiber composite riveted joints and found that the failure occurring in the composite plates began around the rivet hole and the catastrophic failure of these types of joints resulted from fiber tensile failure. Pramanik et al. [19] claimed that placing composite sheet on the top of the aluminum alloy sheet during the riveting formation was good to avoid crack growth. It was reported in Rao's paper [23] that there were two distinctive failure modes for static loading and cyclic loading: (1) the lap-shear and cross-tension joints failed due to rivet pullout of the bottom aluminum sheet in quasi-static loading; (2) in cyclic loading, the lap-shear joints failed due to kinked crack growth in the bottom aluminum sheet, while the cross-tension joints failed due to rivet pulling out of the top carbon fiber reinforced polymer sheet.

Pull-through performance is an important property for rivet joints, which focus on the through-thickness stiffness and strength of the joints. Catalanotti et al. [24] conducted an experimental and numerical study of the pull-through damage in glass-fiber reinforced plastic laminates and concluded that: (1) the type of resin did not affect the mechanical response of the joints when a pull-through test was performed; (2) delamination of the plies was the main failure mechanism. Gray and McCarthy [25] developed an analytical bolt tension model for through-thickness stiffness prediction of the composite joints based on Rize-approximation method, which can predict stiffness well but cannot analyse the stress. Ma [26] studied the effects of temperature, humidity, thickness, fixture clamp length and bolt head diameter on the pull-through strength of the braided composite laminates. Liu [27] found that pull-through ultimate load of the $\pm 45^\circ$ cross-ply laminate was 25% higher than that of

the 0° unidirectional laminate for glass fiber reinforced aluminum alloy laminates.

In this paper, a composite/aluminum riveted joints subjected to pull-through loading was studied. Both experiment and finite element method (FEM) were used to analyse the failure mechanism in terms of load-displacement response, failure modes and damage propagation.

2 Experiment

To investigate the riveting performance of composite skin and aluminum rib of airplane wing box, a pull-through test of the composite/aluminum riveted joints was conducted according to ASTM D7332 standard [28]. As shown in Figure 1, the specimen was composed of a carbon fiber/epoxy composite laminate ($60 \text{ mm} \times 20 \text{ mm} \times 3.0 \text{ mm}$), a 2A12 aluminum alloy plate ($60 \text{ mm} \times 20 \text{ mm} \times 4.0 \text{ mm}$) and a Ti6Al4V titanium alloy ring groove rivet (diameter $d=4.0 \text{ mm}$). The composite laminate, whose volume percentage of the carbon fiber was 60%, has 24 plies with symmetric lay-up $[45/-45/90/90/0/90/0/90/90/-45/45/90]_s$ that yielded laminate thickness of 3.0 mm (single layer nominal thickness was 0.125 mm). The mechanical properties of the composite laminate, cohesive interface between plies, 2A12 aluminum alloy and Ti6Al4V titanium alloy were given in Tables 1, 2, 3. K_n , K_s and K_t are slope of the bilinear traction-separation response for the cohesive element. τ_n^0 , τ_s^0 and τ_t^0 are strength of the cohesive element. G_{IC} , G_{IIC} and G_{IIIC} are fracture toughness.

The composite/aluminum laminated drilling process was conducted on a 3-axis CNC machine tool with carbide twist drill. After drilling, the specimens with middle hole diameter of 4.0 mm (tolerance $0-0.03 \text{ mm}$) were selected and detected by the HCT-800 A-scan ultrasonic damage detector (Onend, China, resolution $>45 \text{ dB}$, frequency $0.4-20 \text{ MHz}$, scanning range $0-10 \text{ m}$) to ensure no delamination in the laminates.

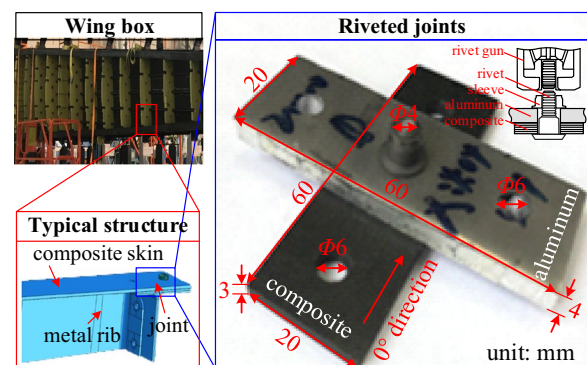


Figure 1 Composite/aluminum riveted joints specimen of airplane wing box

Table 1 Mechanical properties of the carbon fiber/epoxy composite laminate [29, 30]

Mechanical property	Value	Unit
Longitudinal modulus E_1	130	GPa
Transverse modulus E_2 (E_3)	7.64	GPa
Shear modulus G_{12} (G_{13})	3.7	GPa
Shear modulus G_{23}	2.65*	GPa
Poisson's ratio ν_{12} (ν_{13})	0.32	–
Poisson's ratio ν_{23}	0.44*	–
Longitudinal tensile strength X_T	1750	MPa
Longitudinal compressive strength X_C	1850	MPa
Transverse tensile strength Y_T (Z_T)	80	MPa
Transverse compressive strength Y_C (Z_C)	150	MPa
Shear strength S	112	MPa
Density ρ	1.69	g/cm ³

*The value is set according to the transversely isotropic assumption and engineering experience

Table 2 Material properties of the cohesive interface

Material property	Value	Unit
K_n	2170	MPa/mm
K_s (K_t)	835	MPa/mm
τ_n^0	10	MPa
τ_s^0 (τ_t^0)	28.6	MPa
G_{IC}	0.3	N/mm
G_{IIC} (G_{IIIC})	0.6	N/mm

Table 3 Mechanical properties of the 2A12 aluminum alloy and Ti6Al4V titanium alloy

Mechanical property	Aluminum alloy 2A12	Titanium alloy Ti6Al4V	Unit
Elastic modulus E	71.7	108.0	GPa
Poisson's ratio ν	0.33	0.33	–
Density ρ	2.77	4.43	g/cm ³

Experiment set-up of the pull-through test reference to ASTM D7332 standard [28] was shown in Figure 2. Firstly, the composite laminate and aluminum plate were riveted by the titanium alloy ring groove rivet at the middle hole. Secondly, the specimen was fixed to the fixture by fasteners. The fixture was composed by 6 parts, whose diagram was shown in Figure 2, including 2 T-shape plates (Part No. 1 and No. 5), 4 bolts and 4 nuts (Part No. 2 and No. 6), 4 small plates (Part No. 3 and No. 4). Composite laminate (No. 8) was fixed by the upper part of the fixture assembly, including T-shape plate (No. 1), small plate (No. 4) and two fasteners, while aluminum

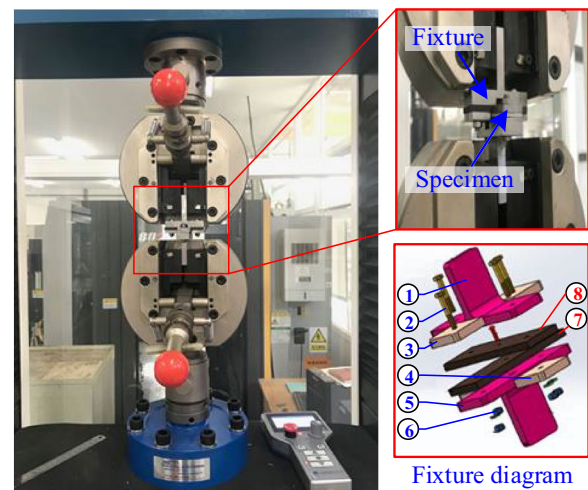
**Figure 2** Experiment set-up of the pull-through test for composite/aluminum joints

plate (No. 7) was fixed by the lower part of the fixture assembly, including T-shape plate (No. 5), small plate (No. 3) and two fasteners. Then the fixture assembly was clamped by the clamping chuck of the DNS100 electronic universal testing machine (Sinotest Equipment, China, maximum allowable load 100 kN, relative error of indication $\pm 0.5\%$). Finally, the tensile load was applied in the form of displacement load with loading speed of 1.0 mm/min. During testing, both displacement and load of the specimen were recorded by the testing machine. The damages of the specimen were observed by the digital microscope VHX-600E (Keyence, Japan, magnification 20 \times to 5000 \times).

Three specimens in total were tested, whose load-displacement curves were shown in Figure 3 with four obvious characteristic stages (first load take-up stage, damage stage, second load take-up stage and failure stage). In Figure 3, slope of the linear load take-up stage represents the stiffness of the specimen, which is 1256.7 ± 61.3 N/mm in average (from 500 N to 2000 N). The first load peak was reached when a continuous crisp cracking sound of fiber breaking was emitted and slight rivet sinking was observed. The first load peak is 2406.4 ± 124.8 N in average when displacement was about 2.0 mm. After the first load peak, it came to the damage stage. Fiber damages and delamination of the composite laminate occurred close to the interface of two plates, which caused suddenly load drop on the load-displacement curves. Rivet sinking produced compressive force around the rivet hole, which has positive effect on preventing further fracture of the fibers so that the specimen could still bear loads, and it came to the second load take-up stage with increase in load. Then it reached the second load peak

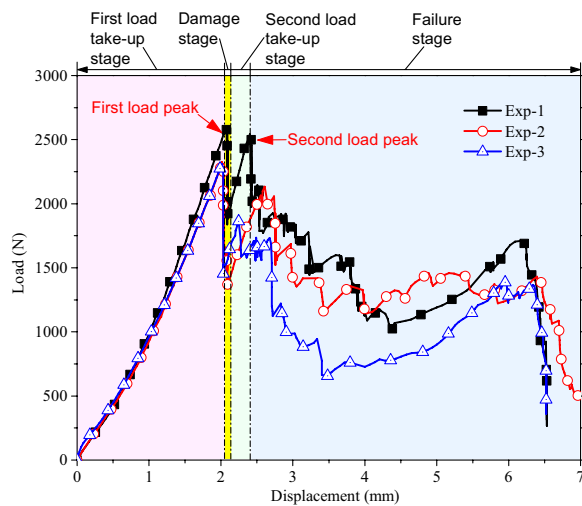


Figure 3 Load-displacement response of the pull-through test for composite/aluminum joints

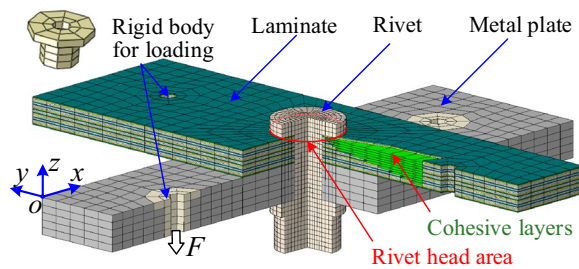


Figure 4 Finite element model of composite/aluminum riveted joints

(2178.8 ± 279.0 N) when a loud sound similar to wood fracture was heard. In mesoscale, location of fiber fracture was random, which results in the differences of the second load peak for different specimens. Since then, with several smaller load decreasing and increasing stages, it came to failure stage and the composite laminate was damaged gradually, especially around the middle hole. At the same time, rivet head began to penetrate the composite laminate, as displacement load increases, the specimen could not bear any load because of serious delamination and rivet-penetration fracture.

3 Finite Element Model

3.1 Finite Element Modelling

In order to investigate the failure mechanism of the composite/aluminum riveted joints, finite element model of composite/aluminum joints was established in Abaqus as shown in Figure 4. Three dimensional 8-node linear reduced integration elements (C3D8R) with enhanced hourglass control method were used for the specimen. After mesh dependence studying

(minimum mesh size ranges from 0.3–1.2 mm), considering the computational cost and results accuracy, in-plane mesh size within the rivet head area (red circle in Figure 4) was set as 0.5 mm for both composite laminate and aluminum plate, while that of other areas were 2.0 mm. There were 5 elements through the thickness for aluminum plate and 24 elements through the thickness for composite laminate. In addition, inserting a cohesive layer between every two layers of composite elements (totally 11 cohesive layers, as shown in Figure 4). Rivet was modelled as a one-piece part with global element size of 0.5 mm.

For convenience and convergence, rigid body method was used to apply boundary conditions. One circle elements within the fastener head of two loading holes of the composite laminate were constrained as a rigid body related to a reference point RP_c , while that of the metal plate were constrained as another rigid body related to another reference point RP_m . Velocity load was applied to the reference point RP_c , which has no other freedoms. All six freedoms of the reference point RP_m were constrained. General contact for explicit analysis with penalty tangential behavior (friction coefficient of 0.1) was used to simulate interaction relationships. In addition, to improve calculation efficiency, mass scaling was used for the whole model based on the restriction that mass changing percent less than 3%.

To reveal the damage propagation mechanism of the composite laminate, progressive damage model based on VUMAT subroutine was used. Hashin-type criteria and cohesive zone method were used to predict the damage initiation and failure modes of the composite laminate. Five kinds of failure modes are considered, which are fiber tensile failure, fiber compressive failure, matrix tensile cracking, matrix tensile crushing and delamination. To predict the initial damage in composites, the linear elastic failure criteria are expressed as follows.

Fiber tensile failure (FT), for ($\varepsilon_1 > 0$):

$$\left(\frac{\varepsilon_1}{X_T/C_{11}}\right)^2 + \left(\frac{\gamma_{12}}{S_{12}/C_{44}}\right)^2 + \left(\frac{\gamma_{13}}{S_{13}/C_{55}}\right)^2 = e_{FT}^2. \quad (1)$$

Fiber compressive failure (FC), for ($\varepsilon_1 < 0$):

$$\left(\frac{\varepsilon_1}{X_C/C_{11}}\right)^2 = e_{FC}^2. \quad (2)$$

Matrix tensile cracking (MT), for ($\varepsilon_2 > 0$):

$$\left(\frac{\varepsilon_2}{Y_T/C_{22}}\right)^2 + \left(\frac{\gamma_{12}}{S_{12}/C_{44}}\right)^2 + \left(\frac{\gamma_{23}}{S_{23}/C_{66}}\right)^2 = e_{MT}^2. \quad (3)$$

Matrix tensile crushing (MC), for ($\varepsilon_2 < 0$):

$$\left(\frac{\varepsilon_2}{Y_C/C_{22}}\right)^2 + \left(\frac{\gamma_{12}}{S_{12}/C_{44}}\right)^2 + \left(\frac{\gamma_{23}}{S_{23}/C_{66}}\right)^2 = e_{MC}^2. \quad (4)$$

Where ε_i ($i=1, 2, 3$) are normal strains, γ_{ij} ($i, j=1, 2, 3$; $i \neq j$) are shear strains, C_{ij} ($i, j=1, 2, 3, 4, 5, 6$; $i=j$) are components of the stiffness matrix. In any of the elements, when the criterion $e \geq 1$ is satisfied, damage variables $d_k=1$ ($k=FT, FC, MT, MC$) will be satisfied, and the element will be damaged by reducing the stiffness matrix as shown in Eq. (5). When there were fiber failure or out-of-plane matrix failure, the element was failed and it will be deleted.

$$\begin{aligned} C_{11}^d &= (1 - d_{FT})(1 - d_{FC})C_{11}, \\ C_{22}^d &= (1 - d_{FT})(1 - d_{FC})(1 - d_{MT})(1 - d_{MC})C_{22}, \\ C_{33}^d &= (1 - d_{FT})(1 - d_{FC})(1 - d_{MT})(1 - d_{MC})C_{33}, \\ C_{12}^d &= (1 - d_{FT})(1 - d_{FC})(1 - d_{MT})(1 - d_{MC})C_{12}, \\ C_{13}^d &= (1 - d_{FT})(1 - d_{FC})(1 - d_{MT})(1 - d_{MC})C_{13}, \\ C_{23}^d &= (1 - d_{FT})(1 - d_{FC})(1 - d_{MT})(1 - d_{MC})C_{23}, \\ C_{44}^d &= (1 - d_{FT})(1 - d_{FC})(1 - 0.9d_{MT})(1 - 0.5d_{MC})C_{44}, \\ C_{55}^d &= (1 - d_{FT})(1 - d_{FC})(1 - 0.9d_{MT})(1 - 0.5d_{MC})C_{55}, \\ C_{66}^d &= (1 - d_{FT})(1 - d_{FC})(1 - 0.9d_{MT})(1 - 0.5d_{MC})C_{66}. \end{aligned} \quad (5)$$

In order to simulate the delamination of the composite laminate, zero-thickness cohesive interfaces were created by offset method with COH3D8 elements. Bilinear traction-separation response was used for cohesive elements during the simulation. Quadratic nominal stress criterion is used to simulate the initiation of the mixed-mode delamination. Once the delamination initiation criterion is met, delamination begins to propagate according to the delamination propagation criterion [31, 32]. Delamination status is represented by the scalar stiffness degradation variable (SDEG), which changes monotonically from 0 (no delamination) to 1 (delamination). The simulation procedure stops as soon as either displacement load is reached or the simulation fails to converge prematurely [33].

3.2 Finite Element Method Validation

In order to validate the proposed FEM based on the Hashin-type criteria and zero-thickness cohesive zone method, typical standard loading tests, including open-hole tensile test according to ASTM D5766 and three-point bending test according to ASTM D7264, were conducted with same materials as described in Section 2, whose stress-strain curves were compared with that of the FEM.

Result comparison of stress-strain curves between the open-hole tensile tests and the FEM are shown in Figure 5(a). It is not necessary to add zero-thickness cohesive layers for open-hole tensile model due to the fact that cohesive layer only affects the mechanical behavior along the out-of-plane direction. In Figure 5(a), average slope value of the stress-strain curves of the open-hole tensile tests is 53241.4 MPa, while that of the FEM is 66149.0 MPa with relative error between the FEM and the tests of 24.2%; average ultimate stress value of the open-hole tensile tests is 563.1 MPa, while that of the FEM is 578.9 MPa with relative error between the FEM and the tests of 2.8%. The slope difference between the FEM and the test is because bump points on the mechanical chucks were hard to embed into composite specimen surface so that there was slight slip of the specimen during tensile test in general. However, the FEM developed in this study did not consider the slip phenomenon. Thus, slopes of experimental curves were lower than that of the FEM curve.

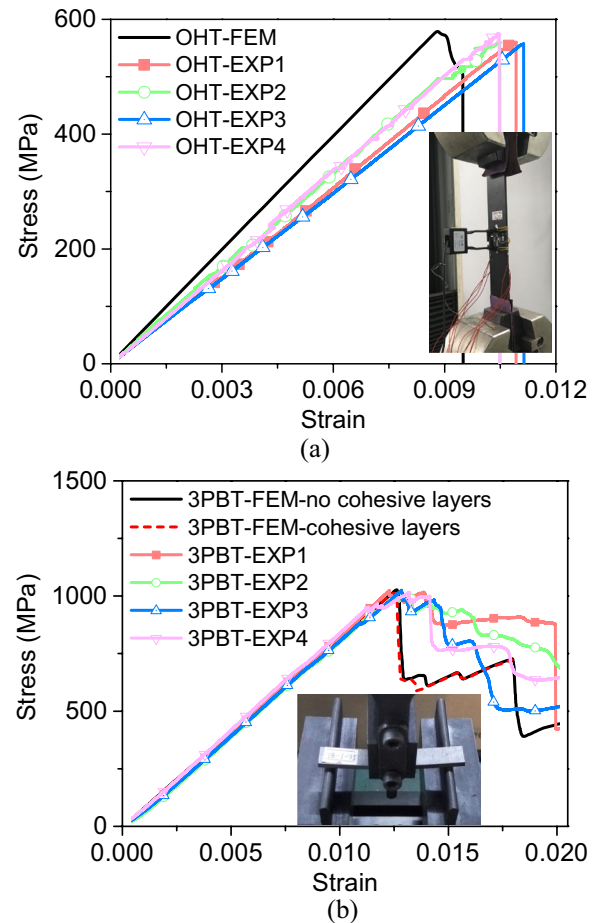


Figure 5 Result comparison of stress-strain curves between the tests and the FEM for: **a** open-hole tensile test; **b** three-point bending test

Result comparison of stress-strain curves between the three-point bending tests and the FEM without cohesive layer and the FEM with cohesive layer are shown in Figure 5(b). In Figure 5(b), average slope value of the stress-strain curves of the three-point bending tests is 84256.5 MPa, while slopes of the FEM without cohesive layer and that with cohesive layer are 81996.6 MPa (−2.7%) and 81973.4 MPa (−2.7%); average ultimate stress value of the three-point bending tests is 1016.3 MPa, while that of the FEM without cohesive layer and that with cohesive layer are 1026.1 MPa (0.96%) and 1021.0 MPa (0.46%). The close simulation results validate that the method of inserting multi-layer cohesive layers has little effect on the load-displacement responses. However, the model with cohesive layers can visualize the delamination between composite plies as an interlaminar fracture phenomenon, while the model without cohesive layers cannot visualize similar phenomenon [4].

It can conclude that the proposed FEM based on the Hashin-type criteria and cohesive zone method is effective to analyse the mechanical behaviors of the laminated composites subjected to tensile or flexural loading.

4 Results and Discussion

4.1 Load-Displacement Response and Predicted Damages

The validated finite element method was then used to analyse the mechanical behavior of the composite/metal riveted joints. The load-displacement curve predicted by the FEM with cohesive layer was compared with that from the experiments, as shown in Figure 6. It can be seen that load-displacement curve from the FEM agrees well with that from the experiments for all 4 characteristic stages exhibited similar trends. The stiffness of the experiments in average is 1256.7 N/mm, predicted stiffness of the FEM is 1359.1 N/mm, and the relative error of

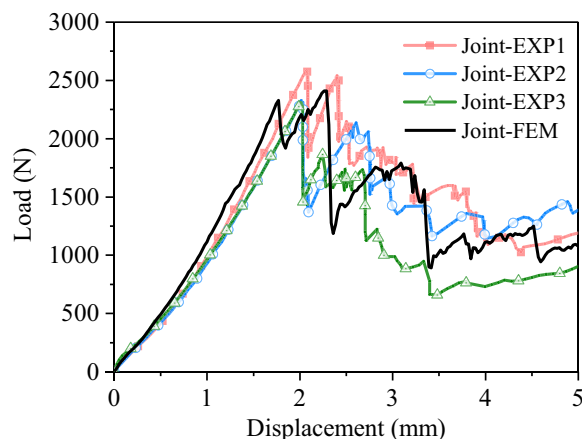


Figure 6 Comparison of load-displacement curves from experiments and finite element method

stiffness between the FEM and experiments is 8.1%. The first peak load of the experiments in average is 2406.4 N, predicted first peak load from the FEM is 2327.7 N, and the relative error of ultimate load between the FEM and experiments is −3.3%. The second peak load of the experiments in average is 2178.8 N, predicted second peak load from the FEM is 2409.9 N, and the relative error of ultimate load between the FEM and experiments is 10.6%. Above results indicate that the proposed FEM is effective to predict the load-displacement response of the pull-through test for composite/metal riveted joints.

Damages of the specimen from the experiment and that from FEM are shown in Figure 7. The experiment specimen was mainly broken by rivet-penetration fracture (Region 1) and delamination (Region 5). There are obviously fiber fracture (Region 2), matrix failure (Region 3) and fiber buckling (Region 4) damages in Figure 7(a). Predicted damages of the laminate from FEM when displacement U_z is equal to 3.4 mm were shown in Figure 7(b). Rivet-penetration fracture, fiber failure, matrix failure, fiber buckling as well as delamination can be seen in Figure 7(b), which have good agreement with experiment results. Figure 7(c) shows the final failure status of the specimen predicted by the FEM ($U_z = 5.0$ mm), in which

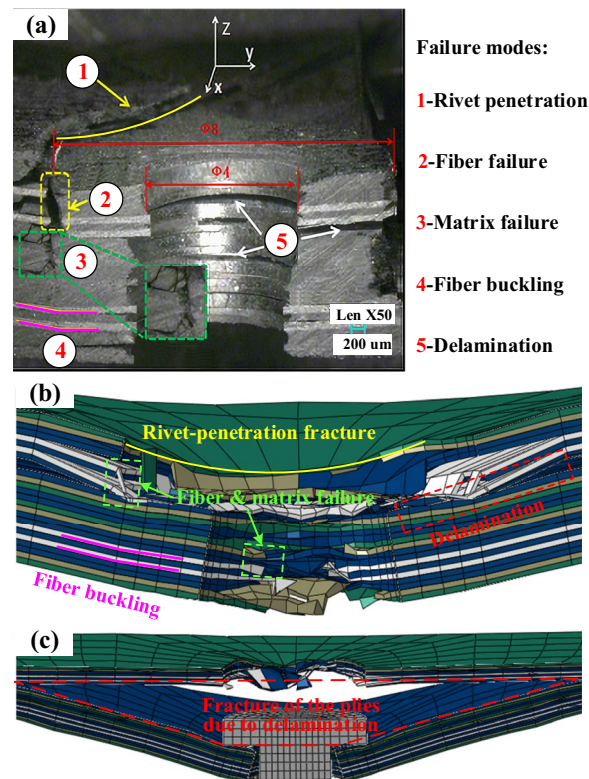


Figure 7 Damages of the experiment specimen and that of the finite element model: **a** damages of the experiment specimen; **b** damages of the FEM; **c** final failure status of the specimen

hole of the composite laminate has been totally broken by rivet head and delamination has been propagated to the whole laminate. The comparison results indicate that the proposed FEM is effective to predict damages of the pull-through test for composite/metal riveted joints.

4.2 Progressive Failure Mechanism of the Joints

Based on the proposed FEM, failure mechanism of the composite/aluminum riveted joints subjected to pull-through loading was investigated.

For first load take-up stage on the load-displacement curve of the FEM, load increases linearly as Uz increases from 0 mm to 0.7 mm, and there are no damages for the specimens. As shown in Figure 8, matrix tensile cracking (MT) firstly appears when $Uz=0.7$ mm, and it propagates rapidly along the radial direction in the ply and along the thickness direction outside the ply. After the first load peak point, matrix tensile cracking has propagated to the transverse edge of the laminate. After the second load peak point, the rivet head penetrates through the top surface of the laminate, and matrix tensile cracking propagates more rapidly and almost reaches its maximum value.

Fiber tensile damage (FT) firstly appears close to the interface between the laminate and the aluminum plate when $Uz=1.1$ mm, and it propagates very slowly. Until the rivet head penetrates through the laminate, fiber tensile damage rapidly propagates at the top surface close to the edge of the rivet head, which is one of the main causes of the suddenly decrease of the load after the second load peak.

Matrix compressive crushing (MC) firstly appears at elements under the edge of the rivet head in the middle plies when $Uz=1.4$ mm. And it propagates slowly to the top surface through the thickness of the laminate. Between the first load peak and second load peak, matrix compressive crushing begins propagating rapidly along the circumferential direction under the edge of the rivet head at the top surface, which is the main cause of the load fluctuation when displacement reaches 2.1 mm.

Delamination (SDEG) firstly appears at interface between ply-4 and ply-5 with small size when $Uz=1.4$ mm. Serious delamination appears at interface between ply-16 and ply-17 as displacement reaches 1.8 mm and propagates very rapidly along the longitudinal direction and transverse direction, which causes the suddenly load decrease after the first load peak. After the second load peak point, multi-layer delamination occurs and propagates, which is the other cause of the suddenly decrease of the load after the second load peak. Then, as the displacement increases from 2.4 mm to 3.0 mm, the rivet head penetrates through the laminate layer by layer and contacts with the lower layer, which contributes to close the interface splits caused by delamination so that load increases to another small peak again. Until displacement reaches 3.4 mm, the rivet head has already penetrated through 8 layers of the laminate, and the laminate is fractured.

After above analysis, dominant failure modes and their locations in laminate was illustrated in Figure 9. The length of the line represents the degree of damage. The longer the line, the more serious the damage. It can be concluded that: (1) the laminate is progressively broken

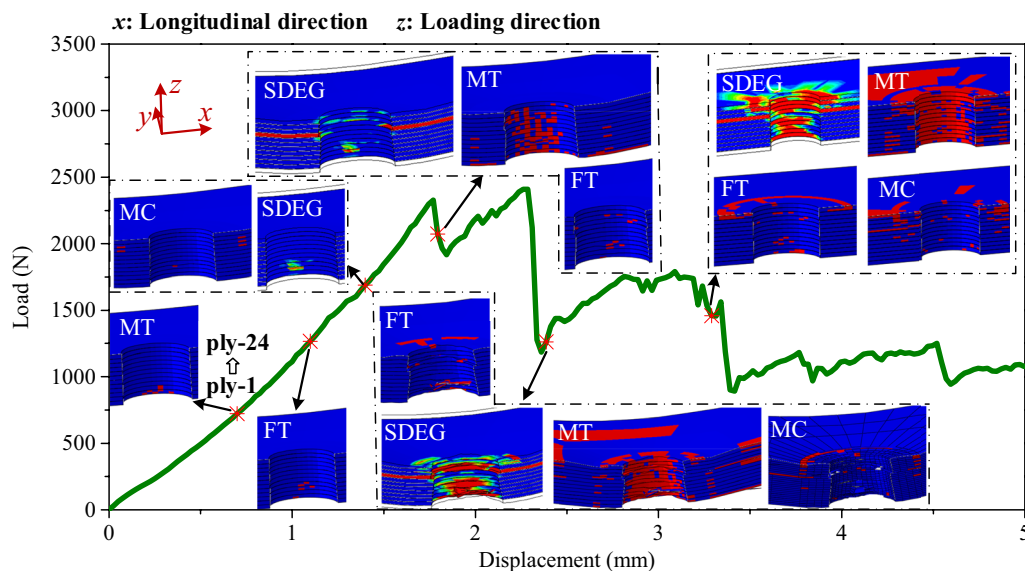


Figure 8 Progressive damage propagation of the specimen from the finite element model

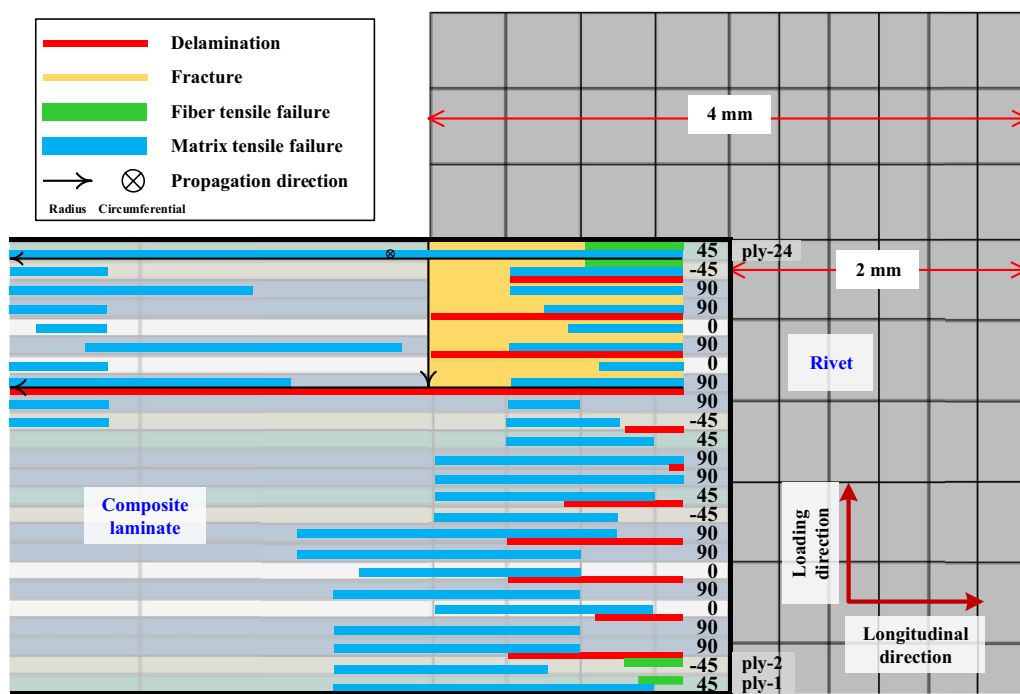


Figure 9 Schematic illustration of dominant failure modes and their locations in laminate

mainly by rivet-penetration fracture and delamination between ply-16 and ply-17; (2) the material within the scope of the rivet head is more dangerous with more serious damages; (3) damages are more serious for the 90° plies than other plies; (4) tensile damages are the main failure modes.

To validate the predicted damage propagation results, three characteristic points ($U_z=1.5$ mm, 2.4 mm, and 3.9 mm) on the load-displacement curve were selected, whose damages were compared with the experiments, as

shown in Figure 10. When $U_z=1.5$ mm, as Figure 10(a) shows, the specimen is in the stage of stiffness and it deforms elastically as the displacement load increases. When $U_z=2.4$ mm, as Figure 10(b) shows, the composite laminate begins to delaminate close to the interface of the composite/aluminum plates due to high tensile stress. When $U_z=3.9$ mm, the rivet has completely penetrated through the top surfaces of the composite laminate, and meanwhile the delamination propagates to the whole laminate. At the three characteristic points, all predicted

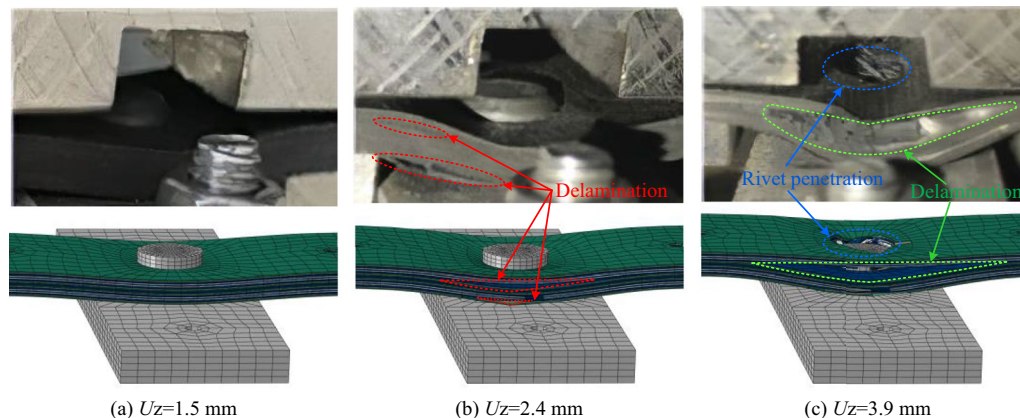


Figure 10 Comparison of damage propagation of the specimens between experiment and finite element model when displacement U_z is equal to: **a** 1.5 mm; **b** 2.4 mm; **c** 3.9 mm

damages from the FEM are in good agreement with the experiment results, which indicates that abovementioned progressive failure mechanism results of composite/metal rivet joints subjected to pull-through loading predicted by the proposed FEM are effective.

5 Conclusions

In this paper, a composite/aluminum riveted joints of airplane wing box subjected to pull-through loading was studied. The specimen consists of a carbon fiber/epoxy composite laminate, 2A12 aluminum plate and Ti6Al4V rivet were tested and their load-displacement responses were analysed according to characteristic points. To predict the damage initiation and failure modes of the composite laminate, a progressive damage model based on the Hashin-type criteria and zero-thickness cohesive zone method was developed using VUMAT subroutine in Abaqus and validated by open-hole tensile test and three-point bending test, which can predict 5 types of failure modes (fiber tensile failure, fiber compressive failure, matrix tensile cracking, matrix tensile crushing and delamination). Load-displacement response, failure modes and damage propagation predicted by the finite element method were all in good agreement with the experimental results for the composite/metal riveted joints. At last, progressive failure mechanism was revealed using the proposed finite element method. Major conclusions are as follows.

- (1) There are 4 obvious characteristic stages (first load take-up stage, damage stage, second load take-up stage and failure stage) on the load-displacement curve for the pull-through test of the composite rivet joints;
- (2) The proposed finite element method can predict stiffness, first load peak and second load peak well with relative error of 8.1%, −3.3% and 10.6% compared to experiment results;
- (3) Specimen was mainly broken by rivet-penetration fracture and delamination between ply-16 and ply-17;
- (4) The material within the scope of the rivet head is more dangerous with more serious tensile damages than other regions, especially for 90° plies.

Acknowledgements

Not applicable.

Author contributions

YY write the article and analysed the data. YB proposed the idea of experiments and assisted to conduct the experiments. XL provided experimental conditions. JW and FD contributed to review the article. All authors read and approved the final manuscript.

Authors' Information

Yuxing Yang, born in 1991, is a PhD at *Marine Engineering College, Dalian Maritime University, China*. He received his doctoral degree from *Dalian University of Technology, China*, in 2019. His research interests include mechanics of composite materials and composite marine propeller.

Yongjie Bao, born in 1980, is a professor at *Dalian Maritime University, China*. He received his doctoral degree from *Dalian University of Technology, China*, in 2010.

Xueshu Liu, born in 1977, is an associate professor at *Dalian University of Technology, China*. He received his doctoral degree from *University of Tokyo, Japan*, in 2012.

Jinlong Wang, born in 1989, is a PhD at *Dalian Maritime University, China*. He received his doctoral degree from *Dalian University of Technology, China*, in 2019.

Fengming Du, born in 1988, is an associate professor at *Dalian Maritime University, China*. He received his doctoral degree from *Dalian University of Technology, China*, in 2016.

Funding

Supported by National Natural Science Foundation of China (Grant Nos. U21A20165, 52205515, 52105431), Applied Basic Research Program of Liaoning Province of China (Grant No. 2022JH2/101300221), Dalian Science and Technology Innovation Fund of China (Grant No. 2022JJ12GX033), National Key Research and Development Project of China (Grant No. 2020YFB2009805), and China Postdoctoral Science Foundation (Grant Nos. 2020M680937, 2020M670734)

Data availability

The data that support the findings of this study are available from the corresponding author upon reasonable request.

Competing Interests

The authors declare no competing financial interests.

Received: 27 January 2021 Revised: 7 June 2022 Accepted: 6 January 2023

Published: 26 January 2023

References

- [1] N Zimmermann, P H Wang. A review of failure modes and fracture analysis of aircraft composite materials. *Engineering Failure Analysis*, 2020, 115: 104692.
- [2] D K Rajak, D D Pagar, P L Menezes, et al. Fiber-reinforced polymer composites: Manufacturing, properties, and applications. *Polymers*, 2019, 11(10): 1667.
- [3] A Katunin, P Sul, A Łasica, et al. Damage resistance of CSA-doped PANI/epoxy CFRP composite during passing the artificial lightning through the aircraft rivet. *Engineering Failure Analysis*, 2017, 82: 116–122.
- [4] Y Yang, X Liu, Y-Q Wang, et al. A progressive damage model for predicting damage evolution of laminated composites subjected to three-point bending. *Composites Science and Technology*, 2017, 151: 85–93.
- [5] G Mittal, K Y Rhee, V Mišković-Stanković, et al. Reinforcements in multi-scale polymer composites: Processing, properties, and applications. *Composites Part B: Engineering*, 2018, 138: 122–139.
- [6] M Li, W Luo, Y Chen, et al. Full-field strain distribution and failure characteristics of CFRP-repaired steel structures. *Engineering Failure Analysis*, 2020, 115: 104664.
- [7] X Meng, Y Huang, Y Xie, et al. Friction self-riveting welding between polymer matrix composites and metals. *Composites Part A: Applied Science and Manufacturing*, 2019, 127: 105624.
- [8] M S H Fatt, D Sirivolu. Marine composite sandwich plates under air and water blasts. *Marine Structures*, 2017, 56: 163–185.
- [9] N Kharghani, C G Soares, N G Tsouvalis. Experimental and numerical study of the bolt reinforcement of a composite-to-steel butt-joint under three-point bending test. *Marine Structures*, 2019, 63: 384–403.
- [10] Y Li, Y Ma, M Lou, et al. Advances in spot joining technologies of lightweight thin-walled structures. *Journal of Mechanical Engineering*, 2020, 56(6): 125–146. (in Chinese)

- [11] H Zhao, J Xi, K Zheng, et al. A review on solid riveting techniques in aircraft assembling. *Manufacturing Review*, 2020, 7: 40.
- [12] B Jiang, Q Chen, J Yang. Advances in joining technology of carbon fiber-reinforced thermoplastic composite materials and aluminum alloys. *The International Journal of Advanced Manufacturing Technology*, 2020, 110(9): 2631–2649.
- [13] A Galińska, C Galiński. Mechanical joining of fibre reinforced polymer composites to metals—A review. Part II: Riveting, Clinching, Non-Adhesive Form-Locked Joints, Pin and Loop Joining. *Polymers*, 2020, 12(8): 1681.
- [14] G Meschut, M Merklein, A Brosius, et al. Review on mechanical joining by plastic deformation. *Journal of Advanced Joining Processes*, 2022, 5: 100113.
- [15] D Krassmann, E Moritzer. Development of a new joining technology for hybrid joints of sheet metal and continuous fiber-reinforced thermoplastics. *Welding in the World*, 2022, 66(1): 45–60.
- [16] C Aldridge. *Riveting technology for carbon fibre and composite material*. Surrey: Mack-Brooks Exhibitions, 2016 [2020-12-21]. <https://www.fastfixtechnology.com/automotive/riveting-technology-for-carbon-fibre-and-composite-material>.
- [17] S D Thoppul, J Finegan, R F Gibson. Mechanics of mechanically fastened joints in polymer–matrix composite structures – A review. *Composites Science and Technology*, 2009, 69: 301–329.
- [18] D Liu, Y Tang, W L Cong. A review of mechanical drilling for composite laminates. *Composite Structures*, 2012, 94: 1265–1279.
- [19] A Pramanik, A K Basak, Y Dong, et al. Joining of carbon fibre reinforced polymer (CFRP) composites and aluminium alloys – A review. *Composites Part A: Applied Science and Manufacturing*, 2017, 101: 1–29.
- [20] S Sathiya Naarayan, D V T G Pavan Kumar, S Chandra. Implication of unequal rivet load distribution in the failures and damage tolerant design of metal and composite civil aircraft riveted lap joints. *Engineering Failure Analysis*, 2009, 16(7): 2255–2273.
- [21] D V T G P Kumar, S S Naarayan, S K Sundaram, et al. Further numerical and experimental failure studies on single and multi-row riveted lap joints. *Engineering Failure Analysis*, 2012, 20: 9–24.
- [22] M Y Solmaz, T Topkaya. Progressive failure analysis in adhesively, riveted, and hybrid bonded double-lap joints. *The Journal of Adhesion*, 2013, 89: 822–836.
- [23] H M Rao, J Kang, G Huff, et al. Impact of specimen configuration on fatigue properties of self-piercing riveted aluminum to carbon fiber reinforced polymer composite. *International Journal of Fatigue*, 2018, 113: 11–22.
- [24] G Catalanotti, P P Camanho, P Ghys, et al. Experimental and numerical study of fastener pull-through failure in GFRP laminates. *Composite Structures*, 2011, 94: 239–245.
- [25] P J Gray, C T McCarthy. An analytical model for the prediction of through-thickness stiffness in tension-loaded composite bolted joints. *Composite Structures*, 2012, 94: 2450–2459.
- [26] W Ma. *Study on the pull-through characteristics of carbon/epoxy braided composite laminates*. Nanchang: Nanchang University, 2016. (in Chinese)
- [27] Y Liu. *Analysis on mechanical properties of glare laminates with countersunk bolted joints subjected to out-of-plane loading*. Harbin: Harbin Institute of Technology, 2018. (in Chinese)
- [28] American Society for Testing and Materials. ASTM D7332/D7332M: Standard test method for measuring the fastener pull-through resistance of a fiber-reinforced polymer matrix composite. PA, West Conshohocken: ASTM International, 2016.
- [29] Y Shen, Y Xiao. Effects of fretting damage on preload relaxation in bolted composite joints. *Acta Materialiae Compositae Sinica*, 2019, 36: 400–409.
- [30] Y He, Y Xiao, Z Su. Effects of surface contact on the dynamic responses of delaminated composite plates. *Composite Structures*, 2019, 229: 111378.
- [31] J F Chen, E V Morozov, K Shankar. Simulating progressive failure of composite laminates including in-ply and delamination damage effects. *Composites Part A: Applied Science and Manufacturing*, 2014, 61: 185–200.
- [32] G Giuliese, R Palazzetti, F Moroni, et al. Cohesive zone modelling of delamination response of a composite laminate with interleaved nylon 6,6 nanofibres. *Composites Part B: Engineering*, 2015, 78: 384–392.
- [33] G Kolks, K I Tserpes. Efficient progressive damage modeling of hybrid composite/titanium bolted joints. *Composites Part A: Applied Science and Manufacturing*, 2014, 56: 51–63.

Submit your manuscript to a SpringerOpen[®] journal and benefit from:

- Convenient online submission
- Rigorous peer review
- Open access: articles freely available online
- High visibility within the field
- Retaining the copyright to your article

Submit your next manuscript at ► [springeropen.com](https://www.springeropen.com)